Applied Surface Science 256 (2010) 3281–3285

Contents lists available at ScienceDirect

Applied Surface Science

journal homepage: www.elsevier.com/locate/apsusc

Engineering the crystal growth behavior: "On substrate" MOD formation of ZnO hollow spheres

Paula A.R. Tafulo [a], Marta Ferro [b], Ariel Guerreiro [a,c], Gerardo González-Aguilar [a,*]

[b] UOSE, INESC-Porto, Rua do Campo Alegre 687, Porto 4169-007, Portugal
[c] CICECO, Departamento de Engenharia Cerâmica e do Vidro, Universidade de Aveiro, Aveiro 3810-193, Portugal
[d] Departamento de Fsica, Universidade do Porto, Rua do Campo Alegre 687, Porto 4169-007, Portugal

ARTICLE INFO

Article history:
Received 23 June 2009
Received in revised form 3 December 2009
Accepted 8 December 2009
Available online 21 December 2009

Keywords:
ZnO
Microstructures
Discontinuous films
Catalysis

ABSTRACT

In this paper is described an easy, one-pot synthesis of ZnO hollow spheres with sizes ranging from 300 nm to 500 nm, by spin-coating deposition on aluminum substrate. Simplified models explaining the shape formation based on film–substrate interaction are discussed. The characteristic size and shape of the nanostructures obtained by the described method and the properties of ZnO as a low-cost biocompatible material make this methodology of synthesis interesting for a wide range of applications including optoelectronics, catalysis and (bio)sensors.

1. Introduction

ZnO is attracting attention as a low-cost material with a variety of exciting applications, ranging from electronics and optoelectronics to medical applications as a biocompatible material. In microelectronics and optoelectronics [1–3], due to its frequent n-type character even in the absence of intentional doping, ZnO is used mainly as a semiconductor or when doped, as transparent conductor electrode (TCE) for photovoltaics, including thin-film solar applications, LCD's and flat panel displays [1,4,5].

Theoretical predictions of room temperature ferromagnetism have promoted ZnO to a potential candidate for applications in spintronics, which is co-substantiated by its recent use in diluted ferromagnetic materials [1,6,7]. Since ZnO is biocompatible, it has long been used in restorative dentistry and orthodontics. Recently, there have been important applications of this material in the fabrication of chemical (bio)sensors [8–10].

ZnO and thin films doped with ZnO have been prepared by several methods including mid-frequency reactive magnetron sputtering [4], electrodeposition [5,7,11–13], chemical vapour deposition (CVD) [14], metallorganic decomposition (MOD or improperly, sol–gel) [15–17] or spray pyrolysis [18]. The use of these techniques create thin films with thicknesses ranging from 500 nm to 1400 nm [11,19,20], and deposition structures with sizes as small as a few nanometres [21,22], thus making ZnO a formidable material to use in nanotechnologies.

The quest to better control the properties of materials and to explore new ways to use them, has stimulated research in many different directions and approaches. The dependence of the materials properties on their size, shape and crystalline structure has promoted the research and development of methods to afford nanostructures [22,23]. Although ZnO is an inexpensive material, many of these techniques are costly, too complex or difficult to be used in large-scale industrial production schemes.

This work is directed to the one-step synthesis and immobilization of ZnO nanostructures with potential use as basis for the development of other applications, such as (bio)sensors or optoelectronic structures composed by hetero layers of inorganic and/or organic materials.

2. Experimental procedures

ZnO precursor solutions were prepared by dissolving ZnO in a mixture nitric acid:acetic acid:water in a 1:2:1 molar relation. Once the solution cleared, ethanol was added to obtain a precursor solution with a concentration of 0.2 M. Commercial aluminium sheets were used as substrates, which were cleaned consecutively with acetone, water and ethanol, each with 10 min sonication.

The solution was then deposited using spin coating at 3000 RPM for 15 s and dried at 150 °C. After completing three deposition-drying steps, the film was heated at 300 ° C to promote phase formation. The microstructure was evaluated using SEM analysis

* Corresponding author.
E-mail address: gaguilar@inescporto.pt (G. González-Aguilar).

0169-4332/$ – see front matter © 2009 Elsevier B.V. All rights reserved.
doi:10.1016/j.apsusc.2009.12.019

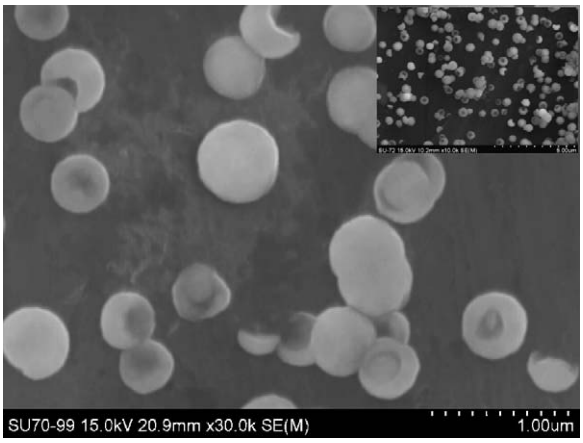

Fig. 1. SEM micrograph of the obtained ZnO nanostructures, inset a more general view illustrating surface coverage.

in a field emission scanning electron microscope Hitachi S-4100. Also, the crystalline structure was verified through X-ray analysis using a Rigaku D-max X-ray diffractometer, equipped with the MDI data scan 3.2 controller software. In order to fix the film to the sample position a small quantity of gum was used.

3. Experimental results

Fig. 1 shows the general aspect of the particles immobilized on the aluminium sheet used as substrate for the sol–gel deposition procedure followed here. As may be noted, the particles have a spherical shape, with approximately 80% being hollow and appearing to be de-capped. The analysis of the distribution of the particle size shows a well defined division: 25% of particles have sizes around 300 nm (±50 nm) while the remaining 75% have sizes around 500 nm (±15 nm). The majority of the de-capped spheres correspond to the bigger spheres (500 nm). The inner spheres have a radius of around 100 nm and the de-capped region corresponds to approximately 40% of the radius of the sphere.

The shape of these spheres is similar to those obtained by Cong and Yu [24], however the particle diameter obtained in this work is very small: (500 nm versus 4000 nm) when compared with those reported in the mentioned work. The diameters of the spheres here obtained are comparable with those obtained by Deng et al. [25]. At the same time, in this work no surfactant was needed to help in the formation of the spheres, contrary to Cong and Yu [24] that used Evans blue-cetyltrimethylammonium bromide or Evans blue as helper in the crystallization process, and Deng et al. [25] who elaborated a procedure to obtain polystyrene core–shell spheres as template in the synthesis of their materials.

The X-ray analysis (Fig. 2) is consistent with the growth of a ZnO structure on an aluminium substrate, as revealed by comparison with the JCPDS-36-1451 card (zincite). However, the pattern of the peaks differ slightly of these obtained by Cong and Yu [24] and Deng et al. [25], but it may be due to the influence of the substrate used in this work. In the referred works the synthesis was made by refluxing, thus obtaining the materials as "free" powders. The broadening of the peaks is an indication of the small size of the particles grown. The EDS results (Fig. 3) also demonstrate the chemical nature of the spheres as being composed by Zn and O, the substrate peak (Al: JCPDS-04-0787) is also observed in the figure as expected.

4. Mechanisms for shape formation

For catalytic purposes it is needed to obtain different discontinuous shapes with high surface areas, like those presented

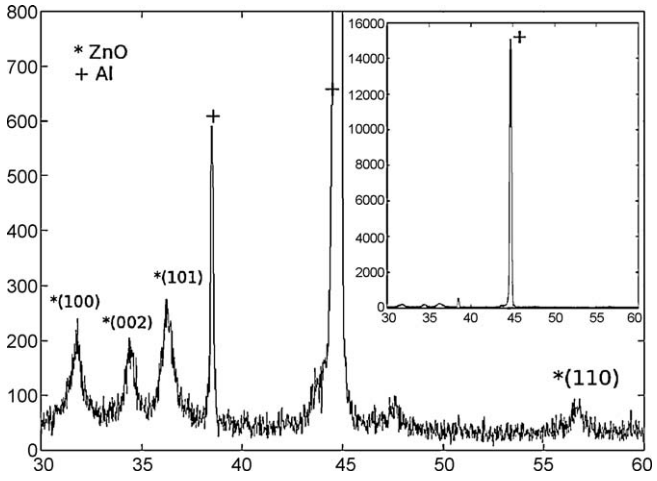

Fig. 2. Details of the X-ray diffractogram demonstrating the existence of ZnO, inset a full scale diffractogram showing the relative importance of the substrate and film peaks.

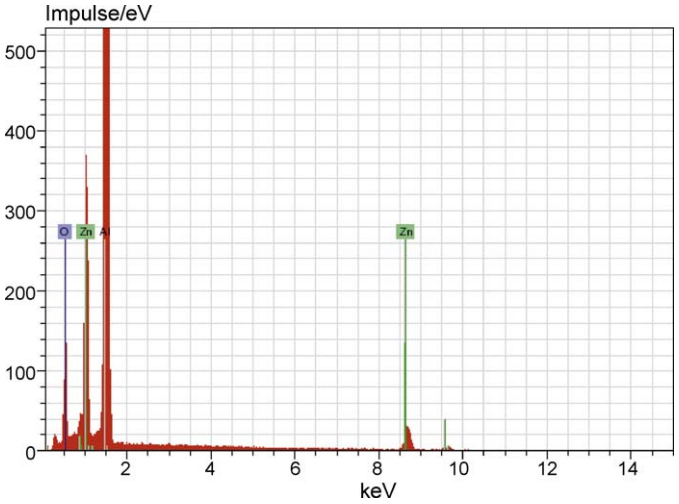

Fig. 3. EDS analysis of the ZnO nanospheres.

here. In the present case the substrate is a good electrical conductor, so this type of structure can be useful for electro-catalytic procedures. However, the mechanism of the shape formation, and consequently the ways to control it, are not well understood, but two hypothesis are being considered:

1. The prepared solution was unable to wet the substrate thus forming microspheres on the substrate surface. Under heating these microspheres dehydrate keeping the shape because the attractive forces in the ZnO pre-crystalline structure are strong enough to avoid the disintegration of the sphere (Fig. 4a).
2. The interaction forces between the aluminum substrate and the ZnO layer are repulsive by nature, breaking the film and forcing the ZnO to adopt the surface configuration with lower energy (Fig. 4b).

Let us examine the causes behind each type of interaction which can be responsible for the formation of the spherical structures.

4.1. Liquid–solid mechanism

During the liquid phase, the prepared solution can be unable to wet the substrate and thus form microspheres. This process is

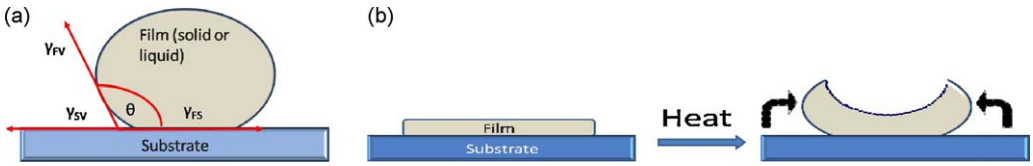

Fig. 4. Models for microstructure formation: (a) non-wetting film (liquid or solid) in contact with a substrate (b) wetting film in which solid–liquid interaction are stronger than the solid–solid interaction of the crystallized film.

determined by the surface and interface energies between the substrate, the liquid solution and the surrounding gas. Experimentally the magnitudes of these energies determine the angle Θ formed at the interface between these phases [26]. The relation between these quantities can be derived from the Newton–Stokes equation [26,28] by imposing mechanical equilibrium at the interface resulting in:

$$\gamma_{SF} = \gamma_S - \gamma_F \cdot \cos\Theta \tag{1}$$

where γ is the surface energy of S (substrate), F (film) and SF (substrate-film phase boundary). A favored interaction occurs when $\gamma_F \geq \gamma_S$ and/or (visibly) $\Theta < 90^\circ$. In the case of a liquid–solid interface; γ_{SF} yields

$$\gamma_{SF} = \gamma_S + \gamma_F - 2\left(\sqrt{\gamma_S^D \gamma_F^D} + \sqrt{\gamma_S^P \gamma_F^P}\right) \tag{2}$$

were the supra-indexes distinguish the dispersive and polar components of the interactions respectively. Equating the previous two equations yields:

$$\cos\Theta = \frac{2\left(\sqrt{\gamma_S^D \gamma_F^D} + \sqrt{\gamma_S^P \gamma_F^P}\right)}{\gamma_F} - 1 \tag{3}$$

Then, when the dispersive and polar interactions between the solid and the liquid are large enough a good wetting is obtained. Oppositely, when one of the phases is polar and the other is apolar, the wettability is strongly decreased.

The measurement of the above referred magnitudes is difficult. However, we can calculate the critical radius for the formation of the droplet on the surface of the substrate.

The critical size of a droplet is determined by the balance between the weight and the surface energy. If the weight is larger than the surface energy per unit surface, the droplet deforms until it collapses into two or more smaller droplets.

To calculate the critical radius we will consider spherical droplets with a flat lower surface corresponding to the interface with the substrate (Fig. 5).

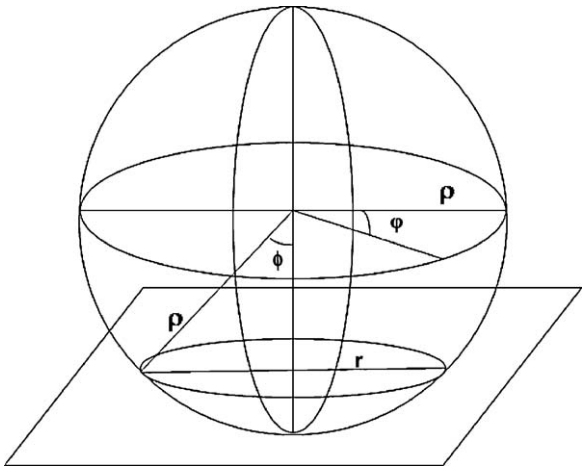

Fig. 5. Geometry of an hypothetical droplet on top of a substrate.

The condition for the existence of such droplet can be expressed as:

$$m \cdot g \cdot \rho \cdot \cos\phi = \pi \cdot r^2 \cdot \gamma_F \tag{4}$$

where m is the mass of the droplet, ρ is the sphere radius, g is the gravity and r is the radius of the surface circle.

r can be calculated as

$$r = \rho \cdot \sin\phi \tag{5}$$

The mass of the droplet is unknown but it can be calculated from the density (d) and the volume of the droplet, the volume can be calculated as:

$$V = \int\int\int \rho^2 \sin\phi \, d\rho \, d\varphi \, d\phi \tag{6}$$

keeping in mind that the variable of interest is ϕ we can use both equations to obtain:

$$2\pi \cdot d \cdot g \cdot \frac{\rho^4}{3} \cos\phi \int_0^{\pi-\phi} \sin\phi \, d\phi = \pi \cdot (\rho \cdot \sin\phi)^2 \cdot \gamma_F \tag{7}$$

approximating $\int_0^{\pi-\phi} \sin\phi \, d\phi$ to $2 \cdot \cos\phi$ and equating yields:

$$\frac{4}{3} \cdot d \cdot g \cdot \rho^2 \cdot \cos^2\phi = \sin^2\phi \cdot \gamma_F \tag{8}$$

reordering

$$\rho = \sqrt{\frac{3 \cdot \tan^2\phi \cdot \gamma_F}{4 \cdot g \cdot d}} \tag{9}$$

Fig. 6 shows the prediction of the critical radius ρ as a function of the contact angle for two distinct situations: $f(x)$ is calculated for pure water ($\gamma_F = 78$ mN/M, $d = 1.0$ g/l), $g(x)$ is calculated for a medium concentration solution, taking as example the parameters of a NaCl 6 M solution ($\gamma_F = 88$ mN/M, $d = 1.4$ g/l) and $h(x)$ is a

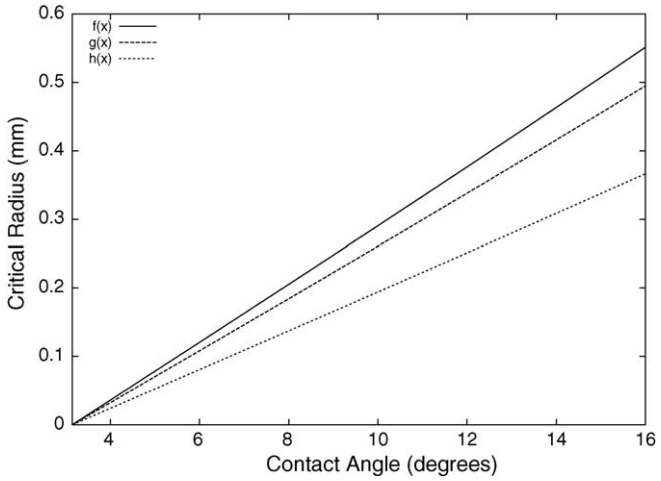

Fig. 6. Restriction for a non-wetting droplet existence: dependence of the calculated critical radius with the contact angle for different conditions: $f(x)$ pure water ($\gamma_F = 78$ mN/M, $d = 1.0$ g/l), $g(x)$ medium concentrated salt solution ($\gamma_F = 88$ mN/M, $d = 1.2$ g/l) and $h(x)$ an "highly" concentrated salt solution ($\gamma_F = 98$ mN/M, $d = 2.4$ g/l).

"highly" concentrated (or semisolid) solution with $\gamma_F = 98$ mN/M, $d = 2.8$ g/l. As can be observed when the concentration and density of the salt increases, the critical radius diminishes. In this way for the $h(x)$ solution, the critical radius for a drop having a contact angle of 5° is around 0.05 mm (50 μm) which is a reasonable quantity for a non-wet film, that after drying and sintering will reduce its volume in a significant amount.

4.2. Solid–solid mechanism

In the case of two solids involved, the Newton–Stokes equations take into account the solid–solid interactions (U_{int}) and the possible strain (U_{strain}) [27]. By analogy with [26], another way to express that relation is:

$$\gamma_{SF} = \gamma_S + \gamma_F - (U_{int} - U_{\text{strain}}) \tag{10}$$

by comparing with (1) and (2)

$$\cos\Theta = \frac{U_{int} - U_{\text{strain}}}{\gamma_F} - 1 \tag{11}$$

Or when the attractive forces (U_{int}) are greater than the energy needed to overcome the mismatch between the lattices forming the interface (U_{strain}), a continuous film will be formed. Oppositely, when the repulsive forces are greater than the attractive ones, it is expected a contact angle θ higher than 90° as indicated in Fig. 4.

As in the previous case parameters like U_{int} and U_{strain} are very difficult to measure, but we can analyze the conditions for the formation of the semi-spherical structures as follows:

The work done to separate the film from the surface is given by the difference between the work needed of forming a new surface and the work needed to separate the film from the substrate, i.e.

$$W_a = \gamma_F \Delta A_{F-Sph} - \gamma_{SF} \Delta A_{SF} \tag{12}$$

ΔA_{F-Sphe} and ΔA_{SF} are the variation of area between the film and the resulting sphere and area of the separated portion of the film. As usual the condition for the spontaneity of the separation process is only fulfilled if $W_a \leq 0$.

For instance, if we consider a final sphere with a diameter $d = 2\rho$), the length of the circumference is $l_{Sph} = \pi \cdot d$ and its area is $A_{Sph} = \pi \cdot d^2$.

For a square piece of film with side length $a = \pi \cdot d$ the area is $A_F = a^2 = \pi^2 \cdot d^2$. The difference of the areas is $\Delta A_{F-Sph} = A_F - A_{Sph} = (\pi^2 - \pi)d^2$.

On the other hand, ΔA_{SF} is expressed as $\Delta A_{SF} = A_F - A_{\text{circ}}$ and $A_{\text{circ}} = \pi(\frac{d}{2} \cdot \cos\phi)^2$ (see Fig. 5).

Resuming, the critical situation is evaluated as:

$$\gamma_F \Delta A_{F-Sph} = \gamma_{SF} \Delta A_{SF} \tag{13}$$

or,

$$(\pi^2 - \pi)d^2 \cdot \gamma_F = \gamma_{SF}(\pi^2 \cdot d^2 - \pi\left(\frac{d}{2}\cos\phi\right)^2) \tag{14}$$

reordering and simplifying

$$\frac{1}{\gamma_{SF}} = \frac{1 - 0.25 \cdot \cos^2\phi}{\gamma_F(\pi - 1)} \tag{15}$$

The most important conclusion of this equation is the fact that the size of the nanostructures are independent of the materials being grown. However, its shape, i.e. the contact angle of the sphere made from a given material is highly dependent of the nature of both the substrate and the material to be prepared.

After analyzing the two cases under study the most probable scenario is that the parameters of the spin-coating process (speed, acceleration and time) control the mass of precursor compounds through limiting the critical radius of the droplet being formed. The contact angle of the final nanostructure is defined at the curing/sintering step by the relation between γ_{SF} and γ_F. However these predictions require an experimental confirmation.

As explained before, the comprehension of these two mechanisms allows one to define strategies for the shape-directed synthesis of a material on a given surface. In the first case (liquid–solid interaction), modifying the wettability of the precursor solution can obtain small or medium size spheres, by controlling the amount of material deposited. However, as the shape is formed as a consequence of solid–solid interactions (second situation), the choice of an adequate dopant will tailor the γ_F and γ_{SF} energies, thus allowing to obtain the desired shape.

5. Conclusion

Small, homogeneously shaped and substrate attached ZnO nanoparticles have been synthesized by an easy to implement and inexpensive technology. The main advantage of this procedure resides in the use of low-cost reagents for the preparation of the precursor solution and relies on deposition using the spin-coating technique, which favors an easy scalability to industrial processing.

The nanoparticles obtained are characterized by a spherical shell shape with sizes in the order of 300–500 nm. These structures have large surface areas and can be used to anchor different inorganic and organic materials, allowing assembly of nanodevices with promising applications in the fields of the (bio)sensors and optoelectronics.

Currently, research work is being carried out to better understand the mechanism of formation of these nanostructures, and the dependency of properties like size, shape and chemical constitution on the synthesis parameters.

References

[1] U. Ozgur, Y.I. Alivov, C. Liu, A. Teke, M.A. Reshchikov, S. Dogan, V. Avrutin, S.J. Cho, H. Morkoc, A comprehensive review of ZnO materials and devices, J. Appl. Phys. 98 (2005) 041301.
[2] E. Rita, E. Alves, U. Wahl, J.G. Correia, T. Monteiro, M.J. Soares, A. Neves, M. Peres, Stability and luminescence studies of Tm and Er implanted ZnO singlecrystals, Nucl. Instrum. Methods Phys. Res. B 242 (2006) 580–584.
[3] J.C. Ronfard-Haret, Electrical and luminescent properties of ZnO:Bi,Er ceramics sintered at different temperatures, J. Lumin. 104 (2003) 103–114.
[4] X. Jiang, F.L. Wong, M.K. Fung, S.T. Lee, Aluminum-doped zinc oxide films as transparent conductive electrode for organic light-emitting devices, Appl. Phys. Lett. 83 (2003) 1875–1877.
[5] A. Goux, T. Pauporte, T. Yoshida, D. Lincot, Mechanistic study of the electrodeposition of nanoporous self-assembled ZnO/eosin Y hybrid thin films: effect of eosin concentration, Langmuir 22 (2006) 10545–10553.
[6] R. Seshadri, Zinc oxide-based diluted magnetic semiconductors, Curr. Opin. Sol. Stat. Mater. Sci. 9 (2005) 1–7.
[7] J.B. Cui, U.J. Gibson, Electrodeposition and room temperature ferromagnetic anisotropy of Co and Ni-doped ZnO nanowire arrays, Appl. Phys. Lett. 87 (2005) 133108.
[8] R. Yakimova, G. Steinhoff, J. Petoral, C. Vahlberg, V. Khranovskyy, G.R. Yazdi, K. Uvdal, A. Lloyd Spetz, Novel material concepts of transducers for chemical and biosensors, Biosens. Bioelectron. 22 (2007) 2780–2785.
[9] X.J. Huang, Y.K. Choi, Chemical sensors based on nanostructured materials, Sens. Actuators B-Chem. 122 (2007) 659–671.
[10] G. Eranna, B.C. Joshi, D.P. Runthala, R.P. Gupta, Oxide materials for development of integrated gas sensors—a comprehensive review, Crit. Rev. Solid Stat. Mater. Sci. 17 (2004) 111–188.
[11] J. Katayama, K. Ito, M. Matsuoka, J. Tamaki, Performance of Cu2O/ZnO solar cell prepared by two-step electrodeposition, J. Appl. Electrochem. 34 (2004) 687–692.
[12] A. Chatterjee, J. Foord, Electrochemical deposition of nanocrystalline zinc oxide at conductive diamond electrodes, Diamond Relat. Mater. 15 (2006) 664–667.
[13] B. Cao, W. Cai, H. Zeng, G. Duan, Morphology evolution and photoluminescence properties of ZnO films electrochemically deposited on conductive glass substrates, J. Appl. Phys. 99 (2006) 073516.
[14] T. Riemann, J. Christen, G. Kaczmarczyk, A. Kaschner, A. Hoffmann, A. Zeuner, D. Hofmann, B.K. Meyer, Microscopic analysis of high quality thick ZnO CVD layers: imaging of growth domains, strain relaxation, and impurity incorporation, Phys. Stat. Sol. (b) 229 (2002) 891–895.

[15] C.H. Bae, S.M. Park, S.E. Ahn, D.J. Oh, G.T. Kim, J.S. Ha, Sol–gel synthesis of sub-50 nm ZnO nanowires on pulse laser deposited ZnO thin films, Appl. Surf. Sci. 253 (2006) 1758–1761.
[16] N. Asakuma, H. Hirashima, H. Imai, T. Fukui, M. Toki, Crystallization and reduction of sol–gel-derived zinc oxide films by irradiation with ultraviolet lamp, J. Sol–Gel Sci. Technol. 26 (2003) 181–184.
[17] S.J. Kwon, J.H. Park, J.G. Park, Selective growth of ZnO nanorods by patterning of sol–gel-derived thin film, J. Electroceram. (2006) 455–459.
[18] A. Maldonado, S. Tirado-Guerra, M. Melendez-Lira, M.L. Olvera, Physical properties of ZnO:F obtained from a fresh and aged solution of zinc acetate and zinc acetylacetonate, Sol. Energ. Mater. Sol. Cells 90 (2006) 742–752.
[19] M. Fahoume, O. Maghfoul, M. Aggour, B. Hartiti, F. Chraibi, A. Ennaoui, Growth and characterization of ZnO thin films prepared by electrodeposition technique, Sol. Energ. Mater. Sol. Cells 90 (2006) 1437–1444.
[20] S.J. Limmer, E.A. Kulp, J.A. Switzer, Epitaxial electrodeposition of ZnO on Au(1 1 1) from alkaline solution: exploiting amphoterism in Zn(II), Langmuir 22 (2006) 10535–10539.
[21] R.M. Nyffenegger, B. Craft, M. Shaaban, S. Gorer, G. Erley, R.M. Penner, A hybrid electrochemical/chemical synthesis of zinc oxide nanoparticles and optically intrinsic thin films, Chem. Mater. 10 (1998) 1120–1129.
[22] E.A. Meulenkamp, Synthesis and growth of ZnO nanoparticles, J. Phys. Chem. B 102 (1998) 5566–5572.
[23] T. Ghoshal, S. Kar, S. Chaudhuri, ZnO doughnuts: controlled synthesis, growth mechanism, and optical properties, Cryst. Growth Des. 7 (2007) 136–141.
[24] H.P. Cong, S.H. Yu, Hybrid ZnO-dye hollow spheres with new optical properties by a self-assembly process based on evans blue dye and cetyltrimethylammonium bromide, Adv. Funct. Mater. 17 (2007) 1814–1820.
[25] Z. Deng, M. Chen, G. Gu, L. Wu, A facile method to fabricate ZnO hollow spheres and their photocatalytic property, J. Phys. Chem. B 112 (2007) 16–22.
[26] A. Rudawska, E. Jacniacka, Analysis for determining surface free energy uncertainty by the Owen–Wendt method, Int. J. Adhes. Adhes. 29 (2009) 451–457.
[27] H. Knozinger, E. Taglauer, Toward supported oxide catalysts via solid–solid wetting, Catalysis 10 (1993) 1–40.
[28] J. Israelachvilli, Intermolecular and Surface Forces, Academic Press, 1995.